Chemical Engineering Journal 157 (2010) 605–619

Contents lists available at ScienceDirect

Chemical Engineering Journal

journal homepage: www.elsevier.com/locate/cej

Influence of mass transfer on gelation time using VIPS-gelation process for chitin dissolved in LiCl/NMP solvent—Modelling and experimental study

D. Bouyer*, L. Vachoud, Y. Chakrabandhu, C. Pochat-Bohatier

Laboratoire Génie des Procédés — Eau et Bioproduits, UMR CIRAD 016, Université Montpellier II, CC 05, place E. Bataillon, 34095 Montpellier Cedex 5, France

ARTICLE INFO

Article history:
Received 16 July 2009
Received in revised form 13 January 2010
Accepted 19 January 2010

Keywords:
Chitin gel
Mass transfer modelling
VIPS-gelation process

ABSTRACT

A non-isotherm mass transfer model is developed for gelation of chitin induced by non-solvent. The system studied in this paper concerns chitin dissolved in LiCl/N-methyl-2-pyrolidone (NMP) at different concentrations ranging from 0.5 to 5% (w/v), and the water as the non-solvent. The gelation is induced by the absorption of water vapours using the vapour induced phase separation (VIPS)-gelation process. The model incorporates coupled heat and mass transfer and due to the very low chitin concentration involved, binary diffusion within the solution was assumed using temperature- and composition-dependent mutual diffusion coefficient. The model was validated using experimental data of gravimetric measurements. The experiments were conducted in a fabrication chamber with controlled process parameters (RH, temperature and air flow conditions) at different chitin concentrations in the initial solution and two temperatures (20 °C and 40 °C). The numerical results were in good agreement with the experimental data, therefore the model has no adjustable parameter for fitting the curves. Then the model was used to predict the composition of the chitin solution at the gelation time, in order to investigate the influence of the non-solvent intake and the solvent extraction involved in the gelation mechanisms. The gelation time was determined by rheological measurements. Results exhibit that the temperature has a great impact on the gelation time through the chitin chains mobility, the interchain association and the mass transfer kinetics. Furthermore, the critical solvent quality that induces the gelation was shown to be correlated to the chitin concentration in the initial solution. Moreover, the chitin chemical structure does not influence the mass exchanges, but the gelation time is reduced using a chitin source characterized by a higher molecular weight and a higher degree of deactylation.

1. Introduction

Chitin and chitosan are copolymers of β,(1 → 4) linked 2-amino-2-deoxy-D-glucan and 2-acetamido-2-deoxy-D-glucan. Chitosan is usually prepared from N-deacetylation of chitin, a naturally occurring polysaccharide, largely widespread in biomass. The term chitosan is attributed to copolymers soluble in dilute acidic media and then to those with a degree of acetylation (DA) below 60%. On the contrary, if the DA overcomes 60% the chitin form prevails.

Potential biomedical applications of chitin have been demonstrated into several areas such as tissue engineering, drug delivery and wound dressings [1–4]. Chitin/chitosan materials can be used in various physical forms such as powders, flakes, and also as gels. Krajewska [5] has previously described the methods used to prepare chitin-based gels and chitin-based membranes: (i) solvent evaporation method [6], (ii) immersion–gelation process for which polymer solution is added to a non-solvent solution, (iii) crosslinking method, (iv) ionotropic gelation method and finally, (v) freeze-drying method.

Chitin is insoluble in many organic or inorganic compounds as well as in water, but soluble in a mixture of N,N-dimethylacetamide (DMAc)/lithium chloride (LiCl) [7] or in a mixture of N-methylpyrrolidinone (NMP)/lithium chloride (LiCl) [8]. The formation of a weak complex between the lithium ions and the hydroxyl functions or the amide groups of chitin leads to the disruption of the hydrogen bondings between polymer chains [9]. Chitin is insoluble and forms gels in water because its structure is stabilized by interchain physical interactions (hydrogen bondings and hydrophobic associations).

It was recently demonstrated [10,11] that two conditions are required for the formation of physical hydrogels from chitin or chitosan solutions. The first condition is relative to the polymer concentration in the initial solution. This concentration must be over the critical concentration of chain entanglements (C^*) because the chain entanglements can form the physical junctions which are required for the formation of a three-dimensional polymer network. The second condition concerns the balance between polymer–polymer interactions and polymer–solvent interactions.

* Corresponding author. Tel.: +33 467 143 327; fax: +33 467 144 787.
E-mail address: Denis.Bouyer@univ-montp2.fr (D. Bouyer).

1385-8947/$ – see front matter © 2010 Elsevier B.V. All rights reserved.
doi:10.1016/j.cej.2010.01.037

This balance must be modified in favour of polymer–polymer interactions in order to decrease the chitin/chitosan solubility. It has to reach a critical value to achieve the sol–gel transition.

Recently, we were interested in the elaboration of physical chitin hydrogels obtained from chitin/NMP(5%LiCl) solutions [12]. In this case, the balance between polymer–polymer interactions and polymer–solvent interactions was modified thanks to the change of the solvent quality of the chitin solution. In other words, the medium surrounding the polymer chains was modified from a good solvent to a bad solvent. The sol–gel transition occurred when a critical amount of non-solvent (water) had penetrated within the chitin solution.

Two processes have been used to generate the contact between the chitin solution and the non-solvent. The first one was the immersion–gelation process which consisted in immersing the chitin solution in a coagulation bath containing pure non-solvent [5,8]. In this case, the gel formation was almost instantaneous because of very rapid mass transfers, i.e. it occurred as soon as the polymer solution came into contact with the non-solvent. This immersion–gelation process is the most commonly used technique to produce chitin gel by contact with aqueous solutions [8,13–16]. We have begun to investigate a second and original process [12]: the vapour induced phase separation (VIPS)-gelation process. In this technique, the chitin gelation was induced by the absorption of non-solvent vapours.

The gels fabricated by the VIPS-gelation process are expected to be more homogeneous in terms of structure since the change in the solvent composition is very progressive [12]. The VIPS-gelation process was shown to induce a slower gelation due to a strong reduction of the mass transfer kinetics comparing to the immersion process for two main reasons: (i) the mass transfer driving force is controlled by gas/liquid equilibrium and (ii) a mass transfer resistance due to gas boundary layer slows down the mass exchanges between the solution and the humid air. Using this process, it was evidenced that the water intake rate was strongly reduced. Besides, the NMP extraction rate was even more affected since its volatility is very low. Only a few papers [17,18] have dealt with the VIPS-gelation process for chitin/NMP(5%LiCl)/water system. This process was actually reported as a step in the experimental procedure to produce chitin scaffolds [18] or chitin film [17]. Nevertheless this step was not fully controlled nor investigated. Recently, the VIPS-gelation process was investigated for the fabrication of chitosan gels, i.e. gels fabricated from the deacetylated form of chitin [19]. In such a case, the gelation has been induced by ammonia vapours, which allowed the deprotonation of chitosan function.

Previously, the VIPS process was used for producing polymeric membranes for many industrial applications. Both experimental and modelling works have been developed to better understand the membrane formation mechanisms and the resulting final morphology. Numerical approaches aim at describing the whole transfer mechanisms during the VIPS process and they integrate the modelling of: (i) the thermodynamic of the polymeric system, involving the Flory Huggins theory, (ii) the external mass exchanges between the cast solution and the humid air and (iii) the internal diffusion into the polymer solution. The first point, i.e. thermodynamic study, needs the knowledge of the interaction parameters between each component of the mixture: solvent/polymer, non-solvent/polymer and solvent/non-solvent. If the interaction parameters are reported in the literature for most systems that involve synthetic polymers, their values are not known for chitin. Furthermore, the diffusion equations that describe the transport phenomena into polymer matrix is quite complex. The free-volume theory developed by Vrentras and Duda (1977) [20] for binary systems and later extended to ternary systems [21] allowed calculating the self-diffusion coefficients in polymer solutions. Nevertheless, 13 independent parameters must be estimated to perform the calculations. Their values are reported for some polymer/solvent/non-solvent systems including synthetic polymers but not for the chitin/NMP/water system. Nevertheless, Vrentras and Duda [22] have reported different methods for determining the self-diffusion coefficients for different systems and they have shown that for very low polymer concentrations, the diffusion coefficients are very close to the diffusion coefficients in pure solvent solution. This condition is quite rare for synthetic system but is more frequent with natural polymer such as chitin.

This paper aims at better understanding and a better controlling the VIPS-gelation process using both experimental and modelling approaches. The gelation of chitin solution was monitored by dynamic rheological measurements and a mass transfer model was developed to predict the variation of the chitin solution composition during the process. To the best of the author's knowledge, neither rheological study nor modelling approach for investigating the mass transfer kinetics was developed in the literature for VIPS-gelation process of chitin/NMP(5%LiCl) solutions. Thus, the mass transfer model developed in this study allows predicting the variation of the chitin solution composition during the gelation process. Mass and heat transfers were coupled via the heat of vapourization due to the water absorption, in order to better describing the external mass exchanges between the solution and the air. The numerical results were validated using experimental data obtained by gravimetric measurements that were performed in a fabrication chamber. Indeed, the gelation process has been conducted in a chamber where the process parameters such as the temperature, relative humidity and air flow rate (i.e. natural convection in the present study) were fully controlled. Two temperatures were tested, 20 °C and 40 C° for two conditions of RH (43 and 75%) and three chitin concentrations: 0% (pure NMP solution), 3 and 5% (w/v). Then, since the gelation mechanism is slow and progressive using this process, it was possible to follow and study the variation of the chitin solution properties as a function of the time. The sol–gel transition was also monitored by rheological measurements in order to estimate the gelation time. The role of the main parameters involved in the gel formation is discussed (temperature, chitin concentration and solvent composition). Finally, the influence of the chitin chemical structure was investigated.

2. Materials and method

2.1. Chitin solution and hydrogel formation

Chitin (degree of acetylation = 76% and viscosimetric molecular weight $\bar{M}_v = 76{,}569$ g/mol, batch 1 from France chitine (Orange, France)), was stored in dry conditions into desiccators where the relative humidity is less than <3%. LiCl was dissolved during 24 h in N-methylpyrrolidinone (NMP), from ALDRICH® (Germany), to obtain a 5% (w/v) LiCl/NMP solution as solvent. Then, chitin was dissolved in this NMP–5%LiCl solution for various concentrations (ranging from 0.5 to 5%, w/v). After complete dissolution, the chitin solution was contacted with water vapours (non solvent) in a fabrication chamber to produce chitin hydrogels. The sol–gel transition occurs when a critical amount of water had penetrated within the chitin/NMP solution.

2.2. Gravimetric analysis

Gravimetric analyses were conducted in-line into a dedicated double-walled chamber (Fig. 1). The diameter and the height of the chamber are equal to 15 cm and 45 cm, respectively. A specific weight of chitin solution (3.7 g) was cast into a 5.65 cm diameter Petri dish, leading to a sample thickness equal to 1.43 mm.

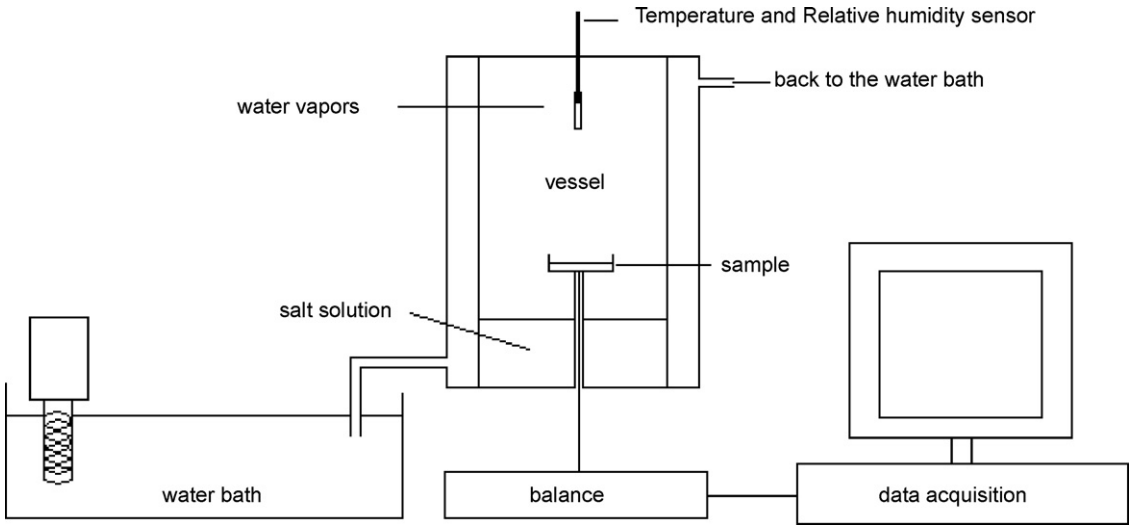

Fig. 1. Schematic of the chamber where the gravimetric measurements were performed.

Then, the chitin solutions were put on a balance Prècisa XB 320 M (0.001 g of precision). The process parameters were controlled in the fabrication chamber: the temperature was adjusted and kept constant (20 °C and 40 °C) using an external heater. The samples were initially heated at the same temperature as the chamber temperature to prevent water absorption at the top solution surface at high temperature (40 °C). The relative humidity (RH) was maintained constant using appropriate saline salt solutions. RH value of 43 and 75% were obtained using the potassium carbonate salt (Sigma–Aldrich) and the sodium chloride salt (Sigma–Aldrich), respectively. A data acquisition system (Balint V.5.00) connected to the balance allowed monitoring the global mass variation during the whole process. During the experiments, the overall mass increase was less than 7%, corresponding to a maximum rising of 0.26 g. However the absolute error on the gravimetric measurements was 5×10^{-4} g, meaning that this weight variation was clearly discriminated.

Furthermore, a statistical analysis was performed to estimate the repeatability of the experiments. The experiments were performed three times for each operating condition, i.e. for the three chitin concentrations (0, 3, 5%, w/v) and the two conditions of fabrication temperature (20 °C and 40 °C). The standard deviation was calculated using the following expression: $\sqrt{(n\sum x^2 - (\sum x^2))/(n(n-1))}$, where n is the number of measurements and x is the mass values obtained at each time step. The results (Fig. 3) exhibit that the repeatability was fairly good for each operating condition and it confirms that the process parameters (temperature, relative humidity and air flow conditions) were well controlled using this fabrication chamber. Therefore, the slight differences between the three curves corresponding to the three chitin concentrations are significant since the standard deviation is weak whatever the temperature.

2.3. Rheometry

Rheological experiments were performed on a rotational controlled stress rheometer (Haake, Rheostress RS 100, Thermo Fisher Scientific) coupled with the Rheowin software. A dynamic mode was used for the rheological monitoring during gelation: it consisted in applying an oscillatory stress to the sample and then in measuring the resulting strain. The plate–plate geometry was used and the diameter of the plates was 20 mm. The gap varied with the sample from 1 mm to 1.5 mm.

The values of the stress amplitude were verified to ensure that all measurements were performed within the linear viscoelasetic region so that the storage (or elastic modulus G') and the loss (or viscous) modulus G'' were independent of the stress. Thus, a stress sweep test at a frequency of 10 rad/s was performed to define this region for both kinds of samples (liquid and gel). Then, from this linear region, an appropriate stress was selected to be as high as possible in order to avoid too low torque. The applied stress varied between 8 Pa and about 100 Pa depending on the physical state of the sample. Using this suitable stress, the elastic and viscous moduli were measured for a constant-stress frequency sweep with frequencies ranging from 0.2 rad/s to 100 rad/s. The temperature of the measurement was controlled by a thermostated bath. The rheometric tests were carried at the temperature of the fabrication chamber (20 °C or 40 °C).

3. Model description

The gelation phenomenon involved during this process is governed by solvent and non-solvent fluxes perpendicular to the polymer solution. Initially, the polymer solution is assumed to have uniform composition, only composed of chitin and NMP (solvent). The polymer concentration is low in our cases, in the range 0–5% (w/v). Once the polymer solution is exposed to humid air, the solvent begins to evaporate. The rate of evaporation is low due to low saturated vapour pressure of NMP. At the same time, the non-solvent intakes the solution due to a gradient of chemical potential between the humid air and the air/solution interface. Therefore a non-isothermal mass transfer will be developed and the heat transfer will be modelled using a lumped parameter approach described in the following paragraphs.

3.1. Description of the geometry

The geometry for mass transfer in this system is presented in Fig. 2. The polymer solution is placed in a Petri dish and exposed to humid atmosphere. In the model formulation, the mass transfer is assumed to be one-dimensional (in the vertical axis) and governed by Fickian diffusion; no diffusion will be assumed in the horizontal axis. Heat transfer will be considered between the bulk gas phase and the sample but uniform temperature within the solution will be assumed. The gas phase next to the top side of the polymer solution is characterized by its temperature T_b (bulk temperature), the relative humidity RH, the partial pressure of each volatile compound

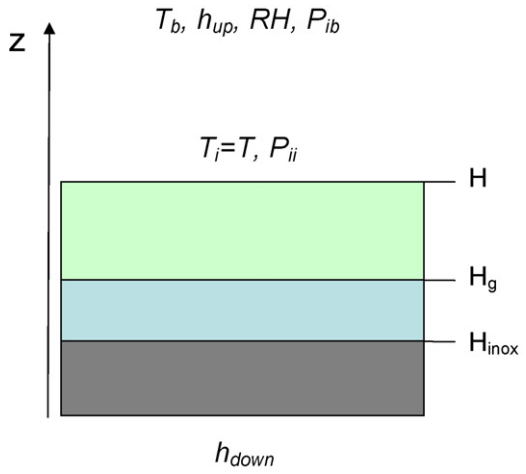

Fig. 2. Schematic of the geometry.

P_{ib}, and the h^{up}. h^{down} characterizes heat transfer coefficient next to the bottom of the Petri dish (glass substrate).

3.2. Mass transfer model

The following assumptions are done for the non-isothermal model: (i) no polymer transfer to the air side, (ii) ideal gas behaviour at the air side and (iii) gas–liquid equilibrium at the air–polymer solution interface. Assuming these assumptions, the model equations are derived as follows:

$$\frac{\partial \rho_i}{\partial t} = \frac{\partial J_i^v}{\partial z} + R_i \quad i = 1, 2 \tag{1}$$

where ρ_i is the mass concentration of component i, defined by:

$$\rho_i = \frac{\phi_i}{\hat{V}_i} \tag{2}$$

ϕ_i and $\hat{V}_i$ are the volume fraction and the partial specific volume of component i, respectively. The subscripts refer to water (1) and NMP (2). R_i represents a chemical reaction term that can be assumed to be null since no chemical reaction is involved between water and NMP neither between the polymer chains of chitin and those solutes species.

The diffusive fluxes J_i^v must be precisely examined in this case. In the case of numerical models that aim calculating mass transfer kinetics within a synthetic polymer solution prior to phase separation, multicomponent diffusivities are usually considered to describe the transport mechanisms. In such cases, the mutual diffusion coefficients can be calculated using different friction based diffusion models [23–25]. Moreover, the knowledge of the self-diffusion coefficients is often necessary. For diffusion phenomena involved within polymer solutions, the free-volume theory developed by Vrentras and Duda [20] is usually used for estimating the values of the self-diffusion coefficients. However, several parameters must be determined such as the critical hole free volume of the components required for a jump, the glass transition temperature of the polymer, the pre-exponential factor, the interaction parameters. For synthetic polymer systems involved in the fabrication of solid membranes, a large literature exists and most parameters are reported or they can be estimated using specific methods [22]. Nevertheless, for natural polymers such as chitin, these data are not available in the literature. Neither the interactions parameters (solvent/polymer, non-solvent/polymer) nor the free-volume parameters have been reported in previous papers and the values of the diffusion coefficients are much more difficult to estimate.

Therefore, another modelling approach was considered for this system. Since the polymer concentration is very low when using the chitin (5%, w/v maximum), it was assumed as a first approach that the diffusion mechanisms were not disturbed by the presence of the polymer chains. Preliminary experiments were performed to focus on the influence of the chitin concentration on the global mass transfer kinetics. Three solutions were prepared in the same Petri dishes, containing the same initial mass of NMP. One Petri dish contained pure NMP solution and the two others contained chitin solutions at 3 and 5% (w/v), respectively. Gravimetric measurements were performed in the fabrication chamber in the same conditions of relative humidity and temperature. The experiments were conducted during 24 h in each case. The temperature and the relative humidity were kept constant using the double shell chamber and appropriate saturated saline solution. The gravimetric curves are plotted in Fig. 3. They clearly point out that the kinetic curves are not strongly affected by the chitin concentration, at least in the range [0–5%, w/v].

Thus, the small molecules of water and NMP were assumed to transfer within the chitin solution as if they were in a NMP/water solution. A Fickian diffusion model was also assumed, which was based on the mutual diffusion coefficient $D_{\text{water/NMP}}$. Note that the diffusion coefficient depends on two parameters: the temperature and the composition of the polymer solution, and more precisely the ratio between the water and NMP concentration. The diffusive fluxes were also expressed as following:

$$J_i^v = D_{ij} \frac{\partial \rho_i}{\partial z} \quad i = 1, 2 \tag{3}$$

Thus, Eq. (1) can be written as follows (subscripts 1 and 2 correspond to water and NMP respectively):

$$\frac{\partial \rho_1}{\partial t} = \frac{\partial}{\partial z}\left(D_{\text{NMP/water}} \frac{\partial \rho_1}{\partial z} \right) \tag{4}$$

$$\frac{\partial \rho_2}{\partial t} = \frac{\partial}{\partial z}\left(D_{\text{NMP/water}} \frac{\partial \rho_2}{\partial z} \right) \tag{5}$$

The mutual diffusion coefficient $D_{\text{NMP/water}}$ depends on the ratio between the NMP and water mole fraction within the solution. Tkacik and Zeman [26] studied the PES/NMP/water system and they reported the expression of the $D_{\text{NMP/water}}$ as a function of the NMP mole fraction in a binary system water/NMP. The expression has been given at 25 °C and the Stokes–Einstein relation allowed calculating the values at 20 °C and 40 °C:

$$D = \frac{kT}{6\pi a \mu} \tag{6}$$

where D is the diffusion coefficient, k is the Boltzmann constant, a is the molecular radius and μ is the dynamic viscosity.

3.3. Initial and boundary conditions

Eqs. (4) and (5) require initial and boundary conditions that can be written as follows:

$$\text{At } t = 0,\ \rho_1 = \rho_1^0 = 0,\ \rho_2 = \rho_2^0 = \frac{1}{\hat{V}_2} \tag{7}$$

$$\text{At } z = 0,\ \frac{\partial \rho_i}{\partial z} = 0\, i = 1, 2 \text{ (symmetry condition)} \tag{8}$$

The boundary condition at the substrate/solution interface, at $z = 0$, corresponds to an impermeable interface for mass transfer:

$$\text{At } z = H,\ \frac{\partial \rho_i}{\partial z} = k_{pi}[P_{ib}(T_b) - P_{ii}(T_i)] \quad i = 1, 2 \tag{9}$$

The Neumann condition at the upper interface involves the continuity of the mass flux at the interface polymer solution/external

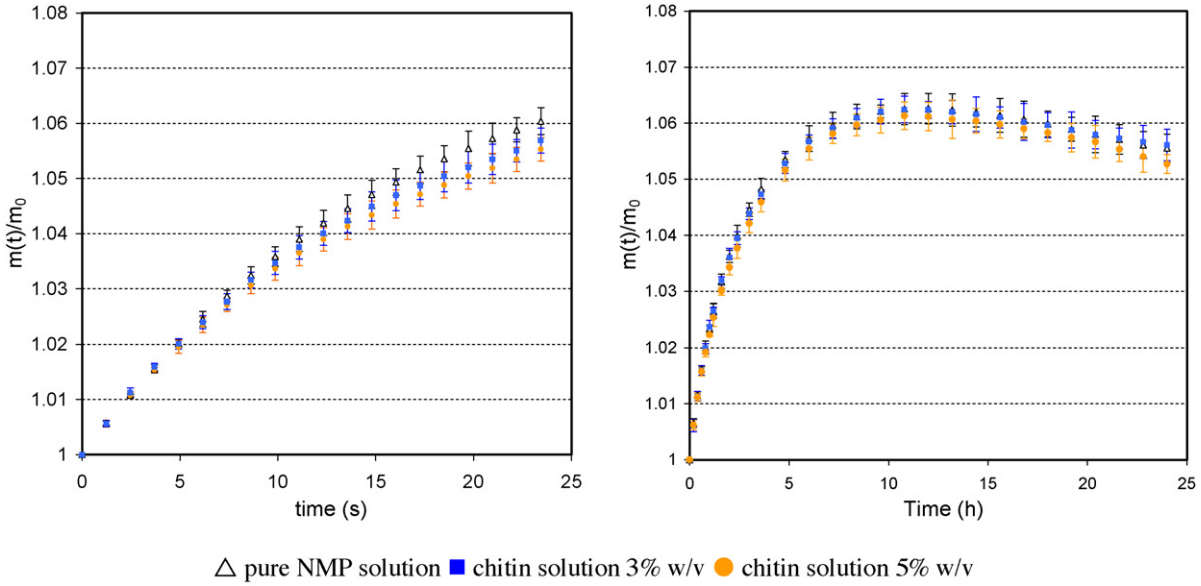

Fig. 3. Comparison between gravimetric curves for different chitin concentrations. $T = 20\,^{\circ}C$ and $T = 40\,^{\circ}C$ for constant RH = 43%. Initial mass = 3.7 g.

Table 1
Value of the parameters of the model.

Parameter	Value
M_1	18 g/mol
M_2	99 g/mol
ΔH_{v1}	2256 J/g
ΔH_{v2}	533 J/g
ρ_1^0	1000 kg/m^3
ρ_2^0	1030 kg/m^3
ρ_3^0	1450 kg/m^3

environment. k_{pi} represents the mass transfer coefficient of component i. The partial pressures of water and NMP in the gas phase are constant during the whole process and depend on the bulk temperature. The local partial pressures at the upper interface depend on both the temperature of the solution and its local composition.

The saturated vapour pressures of solvent/non-solvent were calculated using Eq. (10) [23,25,27,28]. The values of the constants used in the equations are presented in Tables 1 and 2:

$$\log P^{sat} = A - \frac{B}{C+T} \tag{10}$$

where P^{sat} is in kPa and T is in K.

The relation between the partial pressure and the saturated partial pressure for both components are given by the equilibrium curve water/NMP.

3.4. Heat transfer model

Once the mass transfer between the polymer solution and the external environment involves first water absorption and then water evaporation, the local temperature of the solution may change during the process. This could affect the mass transfer phenomena for three main reasons: (i) the partial pressure of both water and NMP directly depend on the air/solution interface temperature. The mass transfer driving force is also affected by a modification of the temperature during the process. (ii) The internal diffusion coefficients depend on the temperature: higher the temperature, lower the viscosity and higher the diffusion coefficients. (iii) The external mass transfer phenomena from the gas phase to the air/solution interface strongly depend on the local temperature, especially if natural convection is involved. In such a case, the difference of the air density between the gas phase and the interface promotes the air motion; therefore it controls the external mass transfer rate. The density difference is directly influenced by the temperature.

Table 2
Values of the constants used in the calculation of the saturated pressure of water and NMP (Eq. (10)).

Parameter	Water	NMP
A	7.942	6.3213
B	1657.5	1709.28
C	227.02	−79.04

Thus, heat transfer must be resolved assuming uniform temperature in the whole thickness of the solution. Indeed the gas-phase convective resistance to heat transfer is much greater than the conductive resistance in the solution and substrate. The Biot number is a non-dimensional number that compares the thermal convective and conductive effect:

$$\text{Biot} = \frac{hLc}{\lambda} \tag{11}$$

where h is the external heat transfer coefficient, Lc is the characteristic length (the film thickness for this modelling problem) and λ is the thermal conductivity of the polymer solution. For this calculation, the NMP thermal conductivity can be considered with regards to its volume fraction within the casting film (>95%). Since the Biot number is lower than 0.01 (4.5×10^{-3} using the most unfavourable case), the heat transfer rate by internal conductivity is much higher than the external heat transfer throughout the air/solution interface, meaning that the heat transfer resistance is located into the gas phase. There is also no internal heat transfer resistance for such thin samples. Besides, strong evaporation or absorption phenomena could appear during the gelation process, due to mass exchanges (solvent extraction and non-solvent absorption). These mass transfer phenomena would lead to local concentration gradients near the air/solution interface since the mass transfer resistance is located within the solution (the solvent and non-solvent molecules diffusion is faster in the gas phase than in the liquid phase). Such mass exchanges would lead to heat production (absorption) or heat consumption (evaporation) at the air/solution interface. Nevertheless, in the case of thin samples, the internal heat transfer along the whole sample thickness performed by heat conduction would

be much faster than the heat production due to mass exchanges. Hence, it would ensure uniform temperature in the whole sample even if heat is exchanged with the external environment. This balance between the heat production and the heat transfer rates explain why no temperature gradient are expected for thin samples, characterized by a Biot number lower than 0.01. Thus, uniform temperature can be assumed along the film thickness. Furthermore, radiative heat transfer is neglected and average values of the density, heat capacity and thermal conductivity are used for the model. The variation of the temperature of the system solution/substrate can be derived as follows, assuming a lumped parameter approach [23,24,29]:

$$\frac{dT}{dt} = -\left[\frac{h_b^{up}(T-T_b) + h_b^{down}(T-T_b) + J_1^v\,\Delta H_{v1} + J_2^v\,\Delta H_{v2}}{\rho_s Cp_s H + \rho_g Cp_g H_g + \rho_{inox} Cp_{inox} H_{inox}}\right] \quad (12)$$

where ρ and Cp are the density and heat capacity, respectively. The subscripts s and g refers to the solution and the glass substrate respectively. ΔH_{v1} and ΔH_{v2} are the vapourization enthalpy of water and NMP, respectively. T is the temperature of the solution and T_b is the bulk temperature, considered to be the same above and below the solution. The initial temperature of the solution was assumed to be equal to the chamber temperature, i.e. 20 °C or 40 °C since the solutions and the casting support were stored at the same temperature prior to the experiments. Furthermore, the assumption of constant chamber temperature during the process was validated by conducting two blank experiments performed at 20 °C and 40 °C and using a thermocouple for monitoring the temperature. Constant values of the temperature with very low deviation were experimentally observed, which confirmed that the double-wall chamber used in these experiments was efficient to maintain constant temperature during a long period.

Note that the model including the coupling between the mass and heat transfer can be applied whatever the thickness of the sample. Besides, for thin samples characterized by Biot numbers lower than 0.01, the lumped parameter approach proposed in the previous paragraph can be used to estimate the variation of the film temperature during time. If the thickness of the casting film would be much higher, the Biot number might exceed 0.01; in such a case, the heat transfer should be simulated within the film and the model architecture would be weakly modified. Indeed, the heat production or consumption would not be immediately balanced by the heat conduction and a temperature gradient would appear within the material. The lumped parameter approach used in this study could not be used for thicker samples.

3.5. External mass and heat transfer coefficients

The external mass and heat transfer coefficients for natural convection can be determined using empirical correlations [28]:

$$\frac{k_{pi} L_c y_{air,lm}}{D_{ig}} \frac{RT}{M_i} = 0.27(GrSc_i)^{0.25} \quad (13)$$

$$\frac{hL_c}{\lambda_g} = 0.27(GrPr)^{0.25} \quad (14)$$

$y_{air,lm}$ is the log mean mole fraction difference of air, λ_g is the thermal conductivity of air, L_c is the characteristic length of the solution surface, Pr, Sc and Gr are the Prandtl, Schmidt and Grashof number respectively, D_{ig} and M_i are the mutual diffusion coefficient and the molar mass of component i in the gas phase, respectively. kp_i is the external mass transfer coefficient. The Prandtl and Schmidt number can be calculated using their standard definitions:

$$Sc_i = \frac{\mu_g}{\rho_g D_{ig}} \quad (15)$$

$$Pr_i = \frac{\mu_g}{\rho_g \lambda_g} \quad (16)$$

D_{ig} can be calculated using the correlation of Fuller et al. [30]:

$$D_{i,air} = \frac{1,43 \times 10^{-7} T^{1.75}}{PM_{i,air}^{0,5}\left[\left(\sum v\right)_i^{1/3} + \left(\sum v\right)_{air}^{1/3}\right]^2} \quad (17)$$

where $M_{i,air}$ is equal to $2(M_i M_{air})/(M_i + M_{air})$, T is the temperature, P is the pressure (bar), M_i and M_{air} are the molar mass of component i and air respectively, and $\sum v$ are the diffusion volume. $\sum v_{water}$ and $\sum v_{air}$ are equal to 13.1 and 19.7 respectively [30] and $\sum v_{NMP}$ can be calculated from the diffusive volume of each atom: $\sum v_{NMP} = 76.74$.

The Grashof number Gr depend on the density gradient between the gas phase and the air/solution interface. Both the temperature and the concentration of the gas phase affect the Grashof number, which can be expressed as following:

$$Gr = \frac{gL_c^3 {\rho_g}^2}{\mu_g^2}\left[-\frac{1}{\rho_g}\left(\frac{\partial \rho_g}{\partial T}\right)_{P,y_i}(T-T_b) - \sum_i \frac{1}{\rho_g}\left(\frac{\partial \rho_g}{\partial y_i}\right)_{P,T}(y-y_i)\right] \quad (18)$$

3.6. Numerical simulation

The non-linear differential partial equations, including coupled mass and heat transfer, were resolved using finite element software (Comsol Multiphysics 3.5®). The one-dimensional geometrical domain was meshed using refined mesh near the solution/air interface since the concentration gradient is expected to be greater in this region; then a geometrical element growth rate was fixed within the domain. The element size was tested to ensure that the numerical results do not depend on the mesh refinement. A variable time step is also assumed for the calculations.

4. Results

The model was first validated using the experimental data obtained in the fabrication chamber. The relative humidity was fixed at 43% and two temperatures were tested: 20 °C and 40 °C. Even though the chitin concentration was assumed not to strongly influence (i) the activity coefficients of both water and NMP and (ii) the transport phenomena within the solution, the simulations were performed at the three concentrations of chitin (0, 3 and 5%, w/v). The slight differences between the curves displayed in Fig. 3 are due to the difference in terms of volume fraction of the polymer. The aforementioned statistical analysis performed on the gravimetric measurements showed that the average value of the standard deviation obtained at each time step was ca. 4×10^{-6} g (0.2% of the mean mass variation). A good repeatability was therefore obtained on the kinetics data for each operating condition since the process parameters were controlled in the fabrication chamber. It is important to note that there is no adjustable parameter in the model presented here; the values of the parameters were calculated using semi-empirical correlations or they were found in the literature. After being validated for different conditions of temperature, the model was used to predict the concentration profiles at the gelation time, which was determined using rheological measurements. It helped focusing on the influence of the solvent quality on the gelation mechanisms.

4.1. Validation of the model

4.1.1. Kinetics curves

Fig. 4 reports the comparison between the simulated and the experimental results. The experimental data were obtained in the

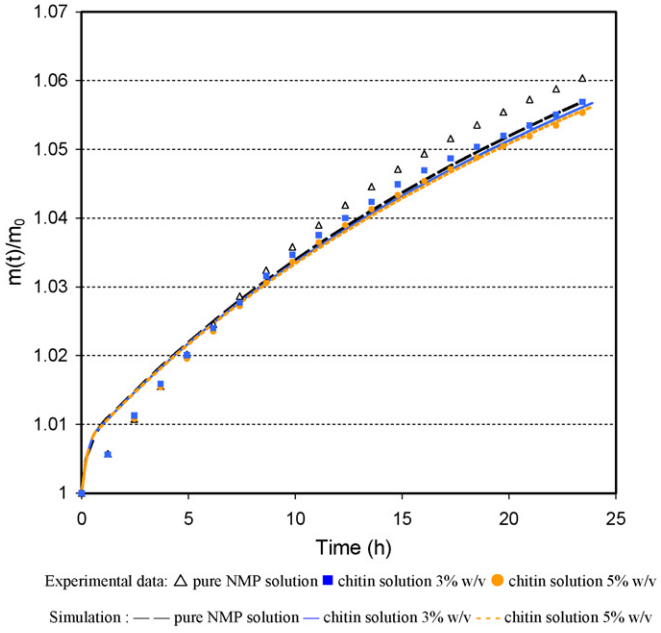

Fig. 4. Comparison between experimental data and simulated results—43% RH and 20 °C.

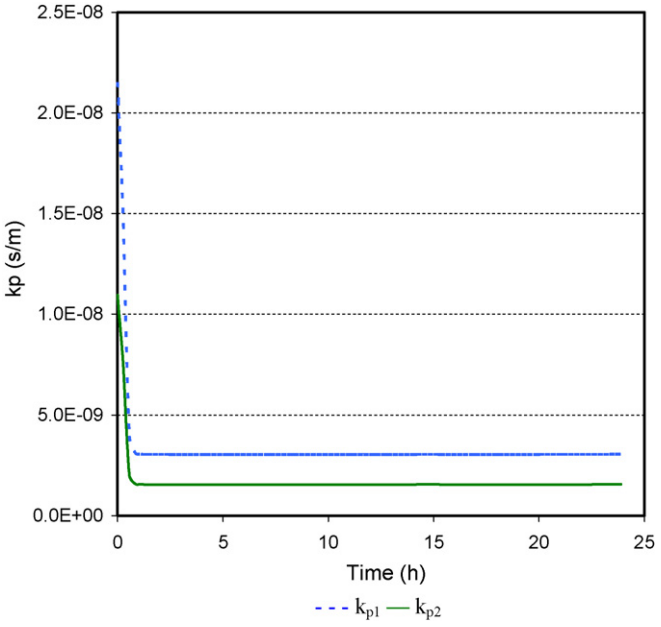

Fig. 5. Variation of the water (k_{p1}) and NMP (k_{p2}) external mass transfer coefficients during time—43% RH, T = 20 °C.

fabrication chamber at 43% RH and 20 °C. In order to clarify the following figures, the standard deviations are not represented when comparing with the numerical predictions. As expected, the kinetic curves do not strongly depend on the polymer concentration since two assumptions were assumed: (i) the activity of water and above all of NMP does not depend on the chitin concentration and (ii) the diffusion rate was assumed to be the same as in a binary NMP/water solution. Fig. 4 exhibits that the agreement between the numerical results and the experimental data is good, especially if we remember that there is no adjustable parameter to fit the curves. Besides, the mass transfer rate is shown to be slightly overestimated at the beginning of the process, during the first 5 h, and more specifically during the first 30 min. The initial mass transfer rate is very high during this short period and then a slope change was suddenly observed. After 30 min, no other slope change was observed until the end of the process. This slope change could be explained by two reasons: (i) a sudden change of the external mass transfer rate or (ii) a modification of the polymer solution properties, which could affect the internal diffusion mechanisms. Since a simple mutual diffusion between NMP and water was assumed within the solution, the first assumption mentioned was retained. For that reason, the variation of the two external transfer coefficients as a function of time was plotted in Fig. 5. Two periods can be easily distinguished: at the beginning of the process, both values of the external mass transfer coefficient of water and NMP reach a maximum and then a sudden decrease was observed. The values of $k_{p\mathrm{NMP}}$ and $k_{p\mathrm{water}}$ were reduced by seven after only 50 min and then their value kept almost constant until the end of the process. For conditions of natural convection, the external mass transfer coefficients depend on the magnitude of the density gradient between the air/solution interface and the gas phase, which can be induced by two effects: (i) a temperature gradient and (ii) a gradient in gas phase composition. During the first minutes of the process, both effects reach their peak since the initial driving force that induces the mass transfer is maximal: at initial time, there is no water within the polymer solution, i.e. its chemical potential is equal to zero. Once the water intakes the solution, its chemical activity and thus its chemical potential increases, leading to a decrease of the mass transfer driving force. The phenomenon is strongly reduced for the NMP since the external atmosphere can be assumed as infinite volume, whose composition does not change during the process. This assumption is all the more relevant for this study that the NMP has a very low vapour pressure whatever the temperature (22 Pa at 20 °C and 106 Pa at 40 °C, cf. Eq. (10)). Thus, the driving force for solvent evaporation can be considered constant during the whole process. Fig. 6 reports the variation of the solution temperature calculated by the model when the chamber temperature is kept constant at 20 °C. Due to exothermic water absorption, the solution temperature increases in the first minutes, besides the temperature gradient between the solution and the gas phase is quite low (less than 1.5 °C). Nevertheless, both effects of temperature gradient and composition difference explain the sudden decrease of the mass transfer coefficients during the first 50 min. Once the amplitude of both effects declined, the

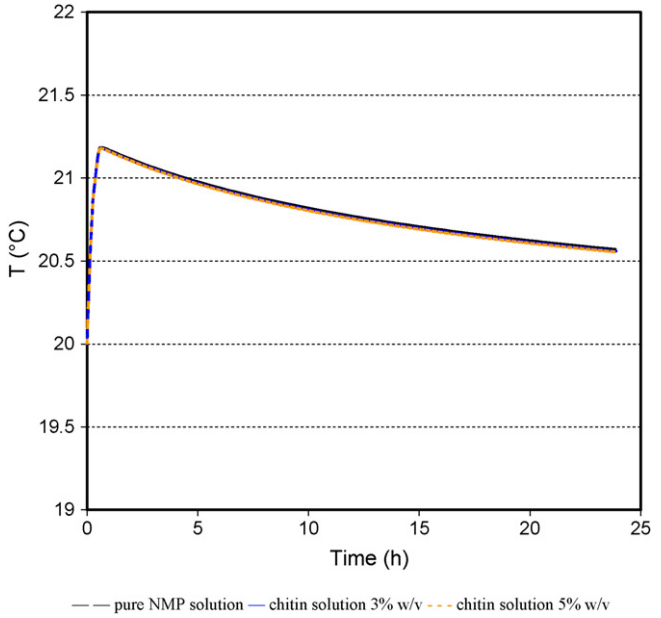

Fig. 6. Variation of the temperature during the process—43% RH and 20 °C.

Grashof number declined as well and the mass transfer coefficients keep a constant value until the end of the experiments.

Then, the mass transfer phenomena were simulated at 40 °C, for the same RH. The results are reported in Fig. 7 for the three concentrations of chitin (0, 3 and 5%, w/v). The simulated curves are in fairly good agreement with the experimental data even though the difference between simulated and experimental curves is higher than at 20 °C. As for the case at 20 °C, a slope change is observed at the beginning of the process. Fig. 9 reports the variation of the solution temperature as a function of time and points out that the temperature gradient was too times higher than at 20 °C, but the time to reach the peak was the same. This peak can also be linked to the sudden decrease of the external mass transfer coefficients reported in Fig. 8. After the slope change, the simulated curves (Fig. 7) kept on increasing until they reached a maximum after 14 h, exhibiting a slight delay comparing to the experimental curves. Then, the global mass started to decrease since the rate of solvent evaporation became larger than the non-solvent intake rate (Fig. 10). A zoom was done on the *y*-axis since the decrease of the fluxes is very strong during the first 30 min. The scale was thus reduced, which makes the analysis easier. Fig. 10 points out that even after 14 h, the water kept on coming into the solution, meaning that the equilibrium state was not reached; thereby the flux was shown to tend to zero at the end of the process (24 h). After equilibrium, it was also expected that the water intake rate would become null and then negative. Indeed, as soon as the solvent evaporates, the water molar fraction in the solution changes and the thermodynamic equilibrium cannot be reached.

In addition, the mass transfer coefficients were shown to have a different behaviour comparing to the previous conditions (T = 20 °C): both of them (for water and NMP) change until the end of the process. The variation of the mass transfer coefficients calculated by the numerical model induces a change in the gravimetric curves: a rapid slow down of the global mass was predicted after the peak was reached. These decreasing rates were shown to be greater than those observed with the experimental data, and the model seems to overestimate the air motion due to the natural convection. This phenomenon is more marked at 40 °C than at 20 °C since the thermal effects due to mass exchanges are higher. It could

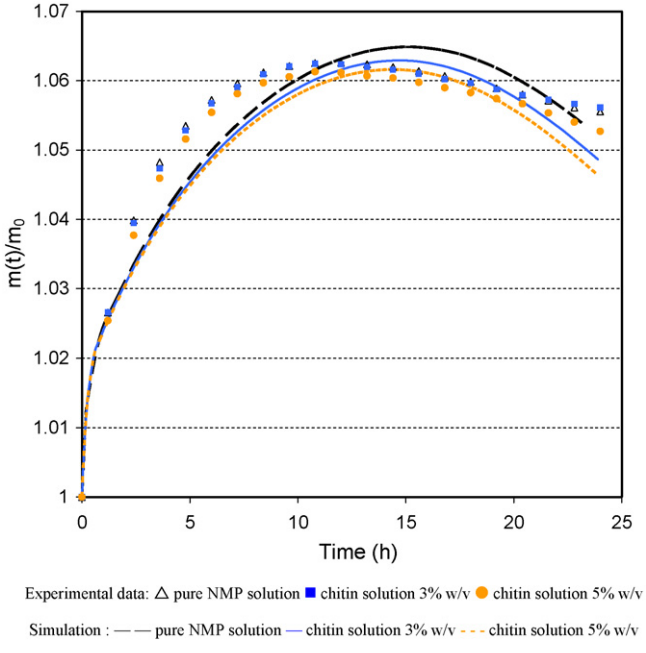

Fig. 7. Comparison between experimental data and simulated results—43% RH and 40 °C.

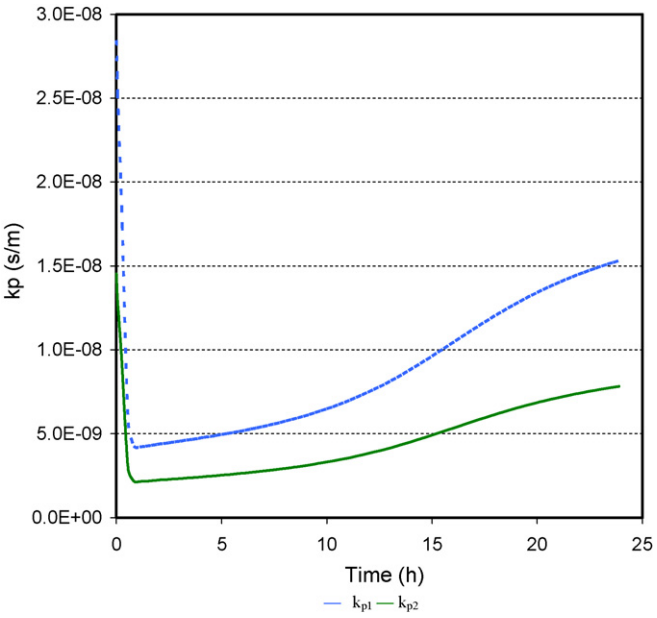

Fig. 8. Variation of the water (k_{p1}) and NMP (k_{p2}) external mass transfer coefficients during time—43% RH, T = 40 °C.

be explained by the specific geometry of the Petri dish containing the chitin solution. Indeed, the simulation was assumed to be one-dimensional and the wall effects were neglected. This assumption is totally relevant for internal mass transfer phenomena, but hydrodynamics above the solution could be affected by the fact that the Petri dish wall is higher than the thickness of the solution. The external mass transfer due to natural convection could be lower than calculated by the numerical model, which considers infinite horizontal plate facing up.

The slight overestimation of the initial external mass transfer coefficients by the model induced a slight difference between the simulated and experimental gravimetric curves. Even if theses deviations were not dramatically strong, it was chosen to test new simulations using constant external mass transfer coefficients.

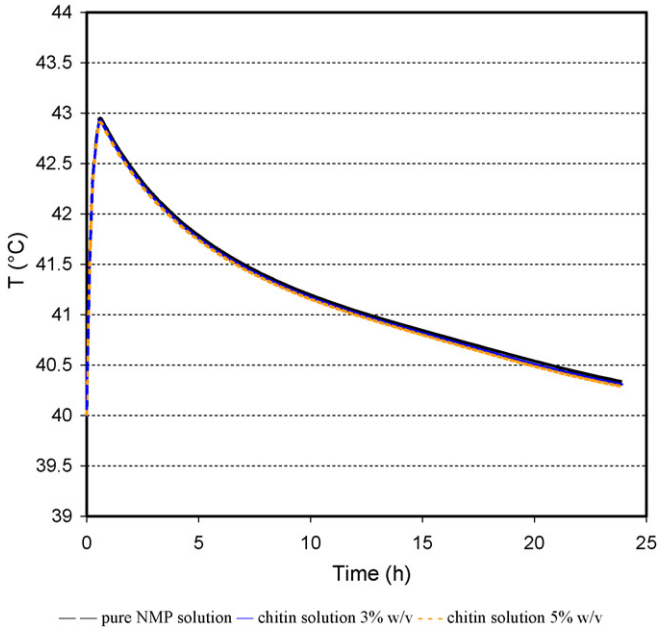

Fig. 9. Variation of the temperature during the process—43% RH and 40 °C.

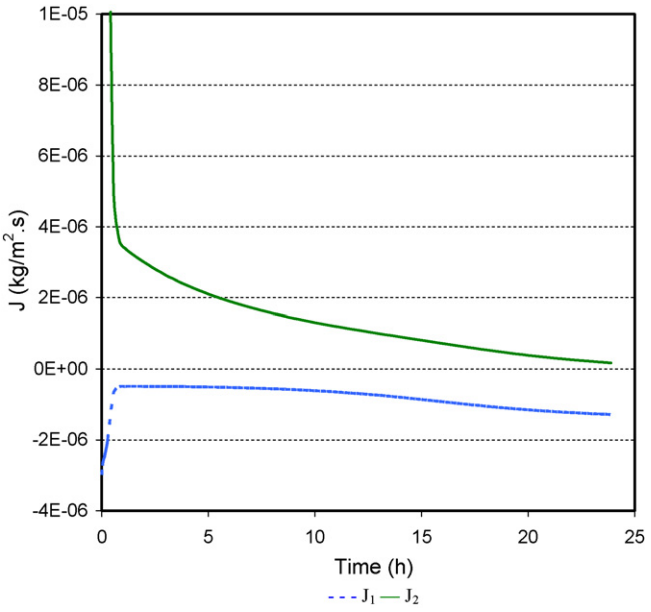

Fig. 10. Variation of the water (J_1) and NMP (J_2) fluxes during time—43% RH and 40 °C.

The values of $k_{p\text{water}}$ and $k_{p\text{NMP}}$ were also chosen from the previous simulated curves, by taking the constant values obtained after 50 min at 20 °C. At 40 °C, time-average values were calculated. The gravimetric curves simulated using constant k_p were reported in Figs. 11 and 12. Both figures exhibit very good agreement between simulated and experimental curves, meaning that these simulations better predict the mass transfer rates between the solution and the gas phase.

4.1.2. Concentrations profiles

Then, the water concentration profiles were plotted versus the dimensionless position (z/H), for each condition of temperature and chitin concentration. Since the chitin concentration was shown to

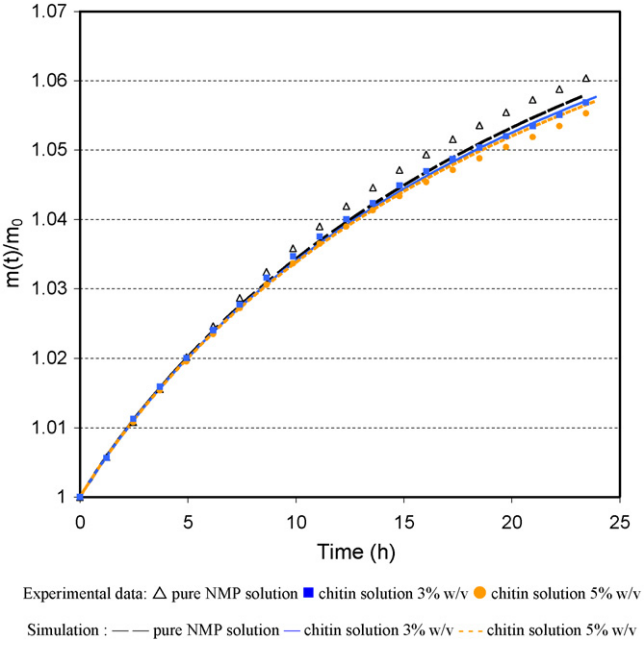

Fig. 11. Comparison between experimental data and simulated results – 43% RH and 20 °C – constant mass transfer coefficient: $k_{p10} = 1.55 \times 10^{-9}$ s/m and $k_{p20} = 3.04 \times 10^{-9}$ s/m.

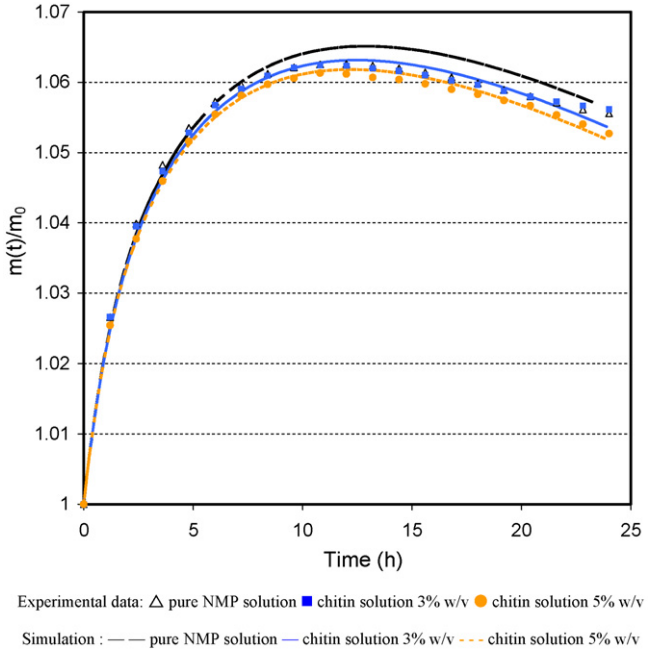

Fig. 12. Comparison between experimental data and simulated results – 43% RH and 40 °C – constant mass transfer coefficient: $k_{p10} = 2.15 \times 10^{-9}$ s/m and $k_{p20} = 4.2 \times 10^{-9}$ s/m.

have a weak influence on the kinetic curves, it was chosen to plot only the curves relative to the highest chitin concentration, i.e. 5% (w/v). The water volume fraction was reported in Fig. 13 at 20 °C and in Fig. 14 at 40 °C.

The variation of the water volume fraction with time is quite different depending on the temperature: after 10,000 s (about 2.8 h), the water concentration was only about 1.5%v at 20 °C but more than 4.5%v at 40 °C. At the end of the process (86,400 s, i.e. 24 h), the water volume fraction was about 6.2%v at 20 °C but about 9.4%v at 40 °C. Besides, whatever the temperature, the concentration profiles clearly exhibit that the gradient of water volume fraction are

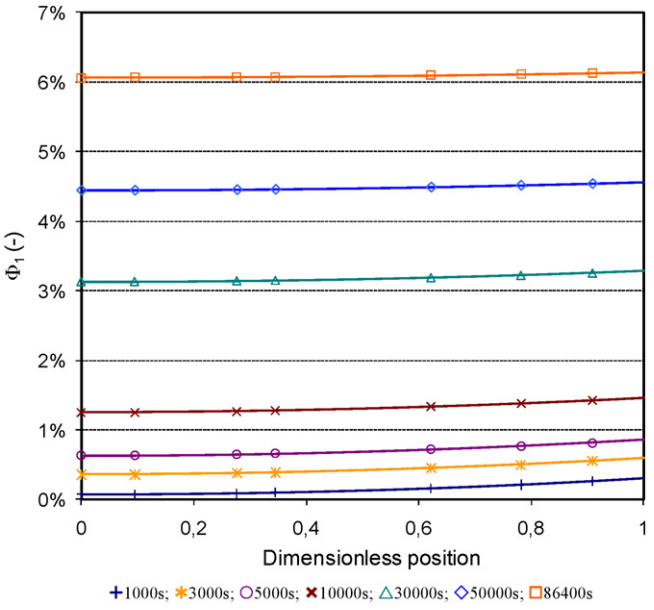

Fig. 13. Concentration profiles (water volume fraction) into the polymer solution during time – 5% (w/v) chitin, 43% RH and 20 °C – constant mass transfer coefficient: $k_{p10} = 1.55 \times 10^{-9}$ s/m and $k_{p20} = 3.04 \times 10^{-9}$ s/m.

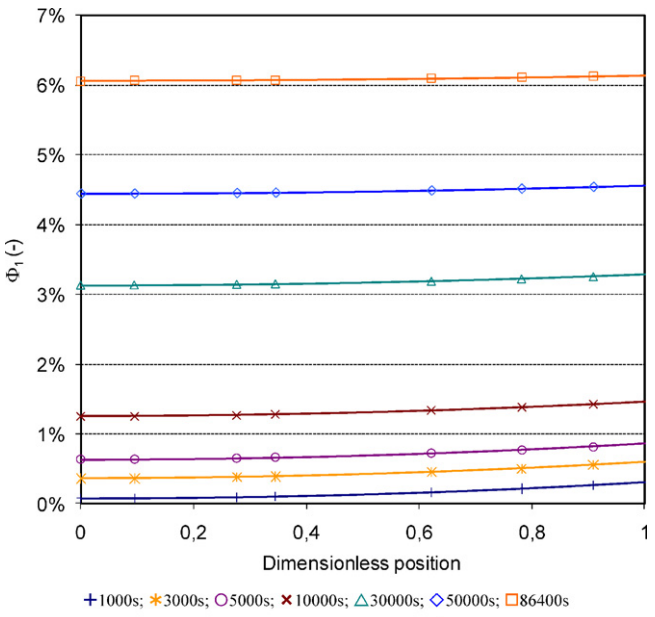

Fig. 14. Concentration profiles (water volume fraction) into the polymer solution during time – 5% (w/v) chitin, 43% RH and 40 °C – constant mass transfer coefficient: $k_{p10} = 2.15 \times 10^{-9}$ s/m and $k_{p20} = 4.2 \times 10^{-9}$ s/m.

weak, leading to flat profiles along the solution thickness. The solvent and polymer concentration profiles were not plotted since they exhibited concentration profiles with very weak gradient due to low mass transfer rates. Besides, the gradients are more pronounced at the beginning of the process, especially at 40 °C, since the driving force to mass transfer is maximal at the beginning of the process, leading to faster external mass exchanges. The gradient of water volume fraction from the bottom to the top of the solution is about 1%v at 40 °C and even lower at 20 °C. It can be concluded that the VIPS-gelation process involves low transfer rates that promote progressive non-solvent penetration in the solution and slow solvent extraction from the solution.

Therefore, developing a numerical transfer model appears crucial for better understanding the mass exchanges involved in the gel formation using VIPS-gelation process. The model can be used for predicting the kinetics of the solvent quality modification, i.e. the molar ratio between the non-solvent and the solvent, or for estimating the concentration gradients within the solution prior to the gelation. The final morphology of the gel could be affected by both effects.

4.2. Use of numerical model for a better understanding of the gelation kinetics

Starting from a homogeneous chitin solution composed of only chitin and its solvent, the gelation phenomenon is induced if the system becomes unstable in terms of thermodynamics. Using this specific system (chitin/NMP), the gelation is induced by the non-solvent intake. For a polymer with a given molecular weight and a given degree of acetylation, the time to achieve the sol/gel transition may be affected by various parameters: (i) the polymer concentration in the initial solution, (ii) the temperature and (iii) the mass transfer kinetics, i.e. solvent extraction rate and non-solvent penetration rate.

In this work, the gelation time was monitored by rheological measurements for increasing chitin concentrations and two different temperatures (20 °C and 40 °C). Using the numerical results on the mass transfer rates obtained by the numerical model presented here, experimental results about gelation time will be discussed.

4.2.1. Procedure for the determination of the gel point

Different procedures have been proposed to measure gelation times [31–33]. One of them consists in placing the sample of the initial solution on the rheometer. In this case, G' and G'' are monitored as a function of the time, for a given frequency (ω). This procedure is easy to perform on a practical point of view, but the rheological characteristics of the sample are observed for only one frequency. This is a major drawback because it was already shown that the gelation time may depend on the frequency used during the measurement [33].

Another technique was considered in this study: the gelation process was monitored by measuring the storage modulus G' and loss modulus G'' as a function of the frequency (ω) at different times during the gelation. This procedure is more time consuming than the first one but it is distinguished by two major advantages:

- The sample is characterized on a wide range of frequencies (or a wide range of solicitation rates) and then it is possible to observe various properties of the sample such as the relaxation of polymer chains.
- The chitin hydrogel is made in the fabrication chamber but not on the rheometer. As a consequence, the mass transfers are better controlled via the process parameters (temperature, RH and air flow natural convection). Furthermore, the geometry of the polymer solution in the fabrication chamber is more convenient for calculating the mass transfer kinetics using the numerical model. Thus, the chemical composition of the sample can be predicted with better accuracy using this experimental procedure.

Several identical samples were prepared with the same weight and the same geometry because these parameters influence the gelation time. They were stored in the reactor in order to induce gelation (relative humidity: 75%, temperature: 20 °C or 40 °C). Then, they were removed from the chamber at different times during gelation and individually loaded on the rheometer platform.

The curves relative to the elastic modulus G' (ω) and the viscous modulus G'' (ω) of a sample stored at different times in the fabrication chamber are reported in Fig. 15 (initial polymer solution of 3%, w/v). A variation of both moduli can be observed. During sol–gel transition, the behaviour of a material changed from that of a liquid

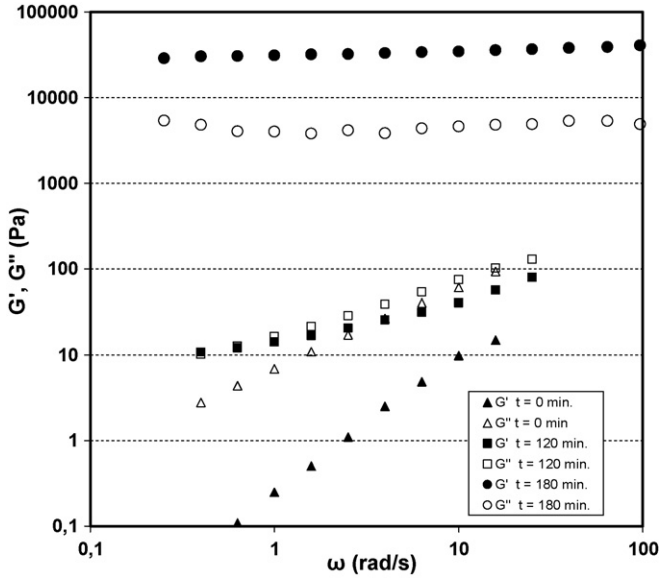

Fig. 15. Variation of G' and G'' versus frequency of a chitin solution for increasing storage time in the fabrication chamber. Polymer concentration in the solution = 3% (w/v). Relative humidity (RH) = 75%. Temperature = 20 °C.

to that of a solid. It is generally considered that when $G' < G''$, the behaviour of the sample was liquid-like, whereas when G' becomes largely over G'', the material behaves like a gel [34–36]. In the case of chitin gel, this transition is clearly evidenced in Fig. 15. For the initial chitin solution ($t = 0$ min), G' was lower than G''. After 180 min of water vapours exposure, G' became higher than G''. This behaviour has to be attributed to the development of physical interactions (hydrogen bonding and hydrophobic interactions) between chitin chains, leading to the formation of a polymer network.

From rheological measurements, it is also possible to distinguish "true" gels from "weak" gels or pseudo-gels [35–37]. For a true or strong gel, G' must exhibit a pronounced plateau extending to an appreciable range of frequencies and must be considerably higher than the loss modulus in this region. "Weak" gels are characterized by a higher dependence to frequency for the dynamic moduli, suggesting the existence of relaxation processes occurring even at short time scales. A lower difference between moduli values is also observed. When the 3% (w/v) chitin solution is exposed during 180 min to water vapour, the value of G' becomes stable and typically one order of magnitude larger than G'' (Fig. 16). Thus, it can be considered that the gel obtained with the VIPS-gelation process is a "true" physical gel in the range of frequency investigated.

Using the procedure described above, gelation kinetics were investigated for various chitin concentrations in the initial solution (ranging from 0.5 to 5%) and for two temperatures (20 °C and 40 °C). The results are reported in Fig. 16 (Table 3.).

4.2.2. *Influence of the temperature on the gelation time*

Fig. 16 clearly indicates that the gelation time decreases on increasing temperature. The gelation process may be affected by the temperature for three main reasons:

- An increase of the temperature promotes the molecular mobility and then it favours the probability of connections between polymer chains, allowing the chitin macromolecules to form physical junction zones more easily.
- As previously demonstrated in the literature [38,39], the temperature plays a major role on low energy interactions involved in the formation of physical polymer network. In the case of chitosan substituted with alkyl chains, the temperature favours interchain associations through hydrophobe–hydrophobe interactions [40].
- Furthermore, as it was shown in the first section of this paper, the temperature strongly affects the mass transfer kinetics between the solution and its external environment. Both the water intake rate in the chitin solution and the solvent removal rate increase when the temperature is raised. Therefore, the critical water content required in the system to induce sol–gel transition is reached more rapidly, leading to faster gelation kinetics.

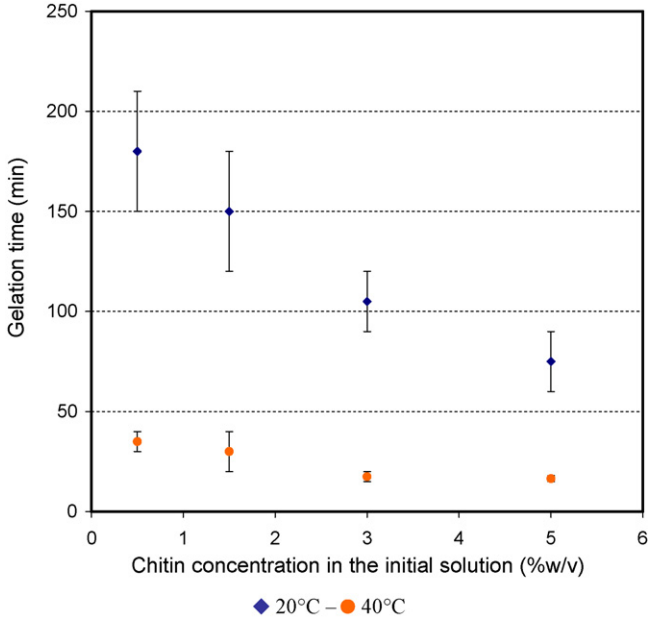

Fig. 16. Influence of chitin concentration in the initial solution and temperature on the gelation kinetics.

Table 3
Nomenclature.

Nomenclature	Unit	Definition
M_1	g/mol	Molar mass of water
M_2	g/mol	Molar mass of NMP
$M_{i,air}$	g/mol	Weighted average molar mass of the component i in the air
M_{air}	g/mol	Molar mass of air
$\sum v$	m^3	Diffusion volume
ρ_i	kg/m^3	Concentration of component i
J_i^v	$kg/(m^2\,s)$	Flux of i
D_{ij}	m^2/s	Diffusion coefficient of i
R_i	$kg/m^3\,s$	Reaction term
ϕ	–	Volume fraction
$\hat{V}_i$	m^3/mol	Molar volume of i
H	m	Polymer solution thickness
H_g	m	Glass substrate thickness
H_{inox}	m	Inox plate thickness
kp_i	s/m	Mass transfer coefficient
h^{up}	$J/(m^2\,s\,K)$	Heat transfer coefficient above the solution
h^{down}	$J/(m^2\,s\,K)$	Heat transfer coefficient below the solution
P_{ib}	Pa	Partial pressure of i in the bulk
P_{ii}	Pa	Partial pressure of i at the solution/air interface
$y_{air,lm}$	–	Log mean mole difference of air
R	8314 J/(K mol)	Ideal gas constant
T	K	Temperature of the solution
T_b	K	Temperature of the bulk
Gr	–	Heat transfer Grashof number
Sc	–	Schmidt number
Pr	–	Prandtl number
λ_g	W/m K	Thermal conductivity of air
P	Pa	Total pressure in the gas phase
β	1/K	Coefficient of volumetric thermal expansion
k	J/K	Boltzmann constant
a	m	Molecular radius
μ	Pa s	Dynamic viscosity of the solution
μ_{air}	Pa s	Dynamic viscosity of gaseous phase
D_{ig}	m^2/s	Diffusion coefficient of component i in the gaseous phase
p^{sat}	kPa	Saturated pressure of NMP and water
ΔH_{vi}	J/kg	Vapourization enthalpy of component i
ρ_s	kg/m^3	Density of the solution
ρ_g	kg/m^3	Density of the Petri dish (glass)
ρ_{inox}	kg/m^3	Density of the inox plate
ρ_{air}	kg/m^3	Density of the air
Cp_s	J/(kg K)	Heat capacity of the solution
Cp_g	J/(kg K)	Heat capacity of the Petri dish (glass)
Cp_{inox}	J/(kg K)	Heat capacity of the inox plate
H_g	m	Thickness of the Petri dish
H_{inox}	m	Thickness of the inox plate
Lc	m	Characteristic length of the system
g	m/s^2	Gravitational acceleration
ν	m^2/s	Cinematic viscosity

To appreciate the impact of the temperature on the mass exchanges, it is interesting to observe, for a given chitin concentration but for different temperatures, the water volume fraction required for gelation. This volume fraction at the gelation time was estimated using the mass transfer model (Table 4 and Fig. 17). Note that the numerical model was validated at 75% RH and the two

Table 4
Average water volume fraction (ϕ_1) and average molar ratio water/NMP (x_1/x_2) required for gelation.

Chitin volume fraction	20 °C		40 °C	
	ϕ_1	x_1/x_2	ϕ_1	x_1/x_2
0.5%	1.8%	9.6%	1.5%	8.6%
1.5%	1.5%	8.2%	1.3%	7.2%
3%	1.0%	5.67%	0.9%	5.0%
5%	0.8%	4.5%	0.8%	4.5%

temperatures (20 °C and 40 °C) by comparing the variation of the global mass of the chitin solution obtained by experiments and the one simulated by the mass transfer model. The global water concentration that is required to induce the gelation was reported in Table 4. Water concentration was displayed in terms of volume fraction. Moreover, the molar ratio between water and NMP (x_1/x_2) was reported at the gelation time, since it represents the solvent quality. The gelation was expected to occur at a critical value of this ratio.

The results exhibit that the amount of water at the gel point was slightly reduced when the temperature was increased. The effect is more pronounced at the lowest chitin concentration (0.5%, w/v) since the time to reach the gelation is higher. Thus, this result confirms that the temperature has an effect on the gelation time, independently on the modification of the mass transfer kinetics due to temperature change. Increasing the temperature affects the chitin chains mobility and favours the polymer gelling properties probably through the polymer–solvent interaction parameter χ_{12}. This result is in good agreement with the study of Vachoud et al. concerning chitin hydrogels prepared by chemical reaction (acetylation of chitosan) [10]. These authors showed that chitin in a given solvent (water–alcohol media) gelled on increasing temperature. This property must be related to the hydrophobic associations of polymer chains, which are favoured by raising the temperature [40].

4.2.3. Influence of chitin concentration

It was observed a slight decrease of the gelation time with increasing the chitin concentration in the range 0.5–5% (w/v), whatever the temperature (Fig. 16). This result has already been reported in the literature for others polymers [41,42]. Since this study aims at distinguishing the role of the main parameters involved in the gel formation, it was interesting to link the solvent chemical composition at the gelation time with the chitin concentration of the initial solution.

Fig. 17 exhibits that the solvent quality (x_1/x_2) required for gelation clearly depends on the chitin concentration. This can be explained by focusing on physico-chemical considerations. During the sol–gel transition, some of the chain entanglements in the initial solution are converted into crosslinks that are responsible for the network formation and for the elastic component of the material. If the chitin concentration increases, the number of entanglements between chitin chains is enhanced leading to more favourable conditions for the formation of physical junctions [11]. Therefore, the solvent quality at the gel point is less modified when increasing the chitin concentration in the initial solution. At the highest chitin concentration (5%, w/v), the amount of water that is necessary to form a gel is about two times lower than for the lowest chitin concentration (0.5%, w/v). This result was pointed out at the two different temperatures.

4.2.4. Gelation front

A gelation front was visually observed on the gel samples during VIPS-gelation process conducted in the fabrication chamber: the gel was shown to form initially at the upper air/solution interface and then to progress from the top to the bottom of the Petri dish. By considering that a critical water content is required to induce the gelation locally and that the gelation mechanisms is rapid comparing to the transfer kinetics, a gelation front may evidence a water concentration gradient into the chitin solution. In order to validate this assumption, the molar ratio x_1/x_2 (water/NMP) was reported at the gelation time for the four chitin concentrations (Figs. 18 and 19) and the two temperatures (20 °C and 40 °C) as a function of the dimensionless thickness. Both figures confirm that concentration gradients exist from the bottom to the top of the chitin solution, leading to the formation of a gelation front. These results can be explained by two reasons: (i) the rates of mass transfer are slow since they are performed by molecular diffusion and (ii) the thickness of the solution is about 1.5 mm. At higher temperature, the gradient is more pronounced: the difference of the ratio x_1/x_2 is two times higher between the bottom and the top surface

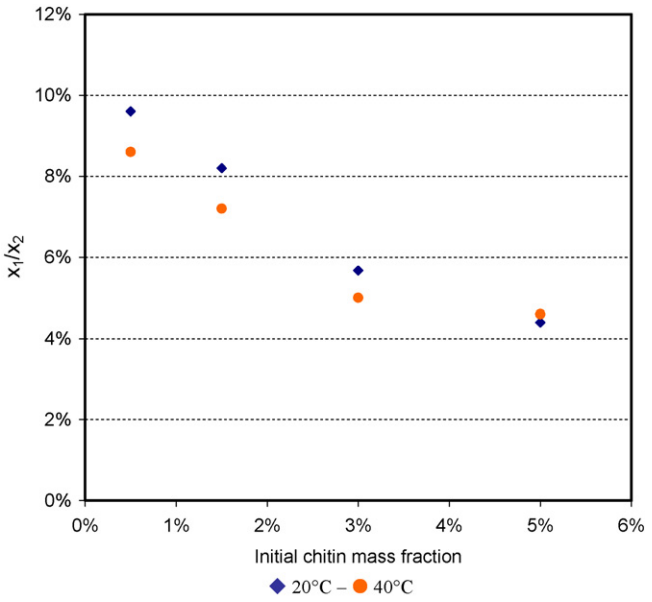

Fig. 17. Molar ratio x_1/x_2 at the gelation time for increasing chitin concentrations (0.5–5%, w/v) – temperature = 20 °C and 40 °C – relative humidity = 75%.

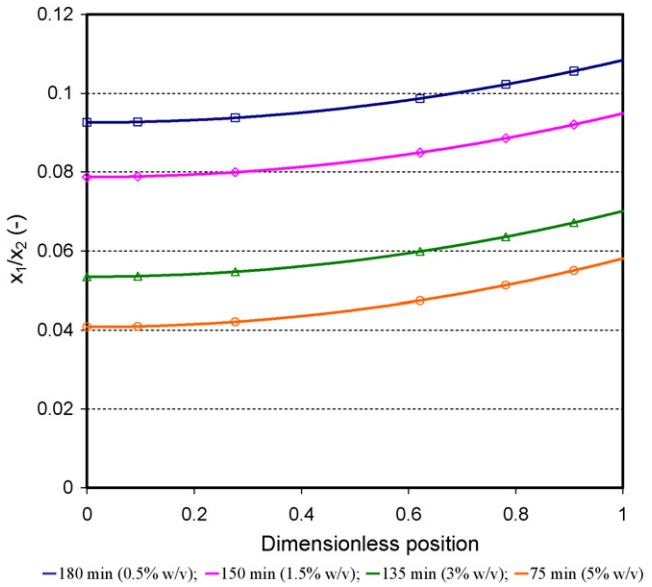

Fig. 18. Profiles of molar ratio x_1/x_2 at the gelation time for increasing chitin concentrations (0.5–5%, w/v) – temperature = 20 °C – relative humidity = 75%.

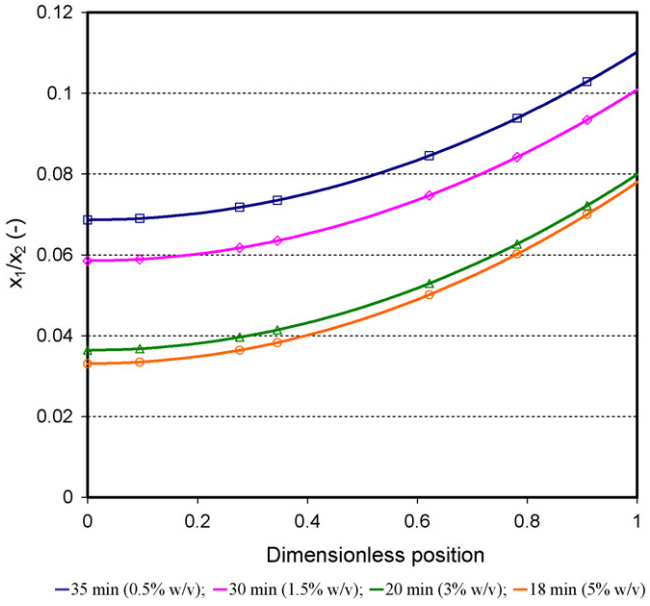

Fig. 19. Profiles of molar ratio x_1/x_2 at the gelation time for increasing chitin concentrations (0.5–5% w/v) – temperature = 40 °C – relative humidity = 75%.

at 40 °C (4%) than at 20 °C (2%), whatever the chitin concentration. This can be explained by the influence of the temperature on mass transfer kinetics: increasing the temperature leads to increase the mass transfer driving force through the partial pressure of the non-solvent. Thus, the external mass transfer resistance is strongly affected by a temperature change whereas the temperature influence on the internal diffusion within the solution is weaker. It leads to an accumulation of non-solvent in the upper region of the solution and then to the formation of concentration gradients.

4.3. Influence of the chitin source on the kinetic curves and the gelation time

In order to appreciate the influence of the chitin chemical structure on the kinetics curve and on the gelation time, additional experiments were carried out with another chitin batch (batch 6 from France Chitine (Orange, France)). This batch was characterized by a higher degree of acetylation (88%) and a higher viscosimetric molecular weight ($\bar{M}_v = 696{,}000$ g/mol) than the batch 1. Concerning this batch 6, it was not possible to monitor gelation time for chitin concentration over 0.3% (w/v) because in this case, rheological behaviour of the initial chitin solution (without addition of non-solvent) is that of a "weak" gels or a pseudo-gel. As a consequence, the mass transfer kinetics and the gelation time were investigated for a polymer concentration of 0.3% (w/v) i.e. lower than the polymer concentrations used for the batch 1.

4.3.1. Kinetic curves

The gravimetric measurements were conducted for this additional chitin solution using the same operating conditions as previously mentioned: 43% RH at two different temperatures (20 °C and 40 °C). The experiments were done three times to include a statistical analysis, which is represented by the standard deviation calculated at each time step. Even if the gelation time was expected to be low in each case, especially at 40 °C, the gravimetric experiments were conducted during a longer duration to compare the experimental data to the model predictions on the weight variation. Fig. 20 reports this comparison for both conditions of temperature. The comparison between Fig. 20 and Fig. 3 exhibits that the global kinetic curves are very similar whatever the chitin source. Indeed, the external process conditions were kept identical (RH, temperature, and air flow conditions), hence the internal mass transport rate of solvent and non-solvent was assumed to be purely controlled by Fickian diffusion; lower the chitin concentration, higher the solvent volume fraction, meaning that at such low chitin concentrations, the polymer chains were not expected to disturb the transport of the small molecules (water and NMP) through the polymeric matrix. It was previously exhibited that the global mass transfer rates were almost identical in the range [0–5%, w/v] for the first chitin source. Since the chitin concentration cannot exceed 0.3% (w/v) using the new chitin source, it is not surprising to obtain similar kinetic curves.

The comparison between the experimental data and the numerical predictions points out different behaviours depending on the temperature. At 20 °C, the agreement between both curves is good during the whole process (50 h in this case). Nevertheless, at 40 °C, a deviation can be observed after 30 h of experiments. The numerical model underestimates the global weight during the second part of the experiments, which corresponds to an evaporation stage of both the solvent (NMP) and non-solvent (water). During this drying period that follows a mass intake period, the drying rate is overestimated by the model. This deviation could be explained by the model assumption made on the solvent vapours. Indeed, the model assumed no solvent vapours in the gas phase during the whole process because of the very low NMP volatility. Whereas this assumption is relevant during a long period, an accumulation of NMP in the gas phase due to its evaporation could have an impact of the mass exchanges after a very long duration. In such a case, the presence of NMP vapours would lead to an increase of the NMP vapour pressure in the gas phase, leading to decrease the driving force to NMP evaporation. Since the NMP evaporation was shown to overcome the water transfer during the second period of the experiments, the experimental global kinetic curve would decrease more slowly than predicted by the model (cf. Fig. 20). This deviation could be corrected taking into account the accumulation of NMP in the gas phase, nevertheless such estimation is very problematic in this

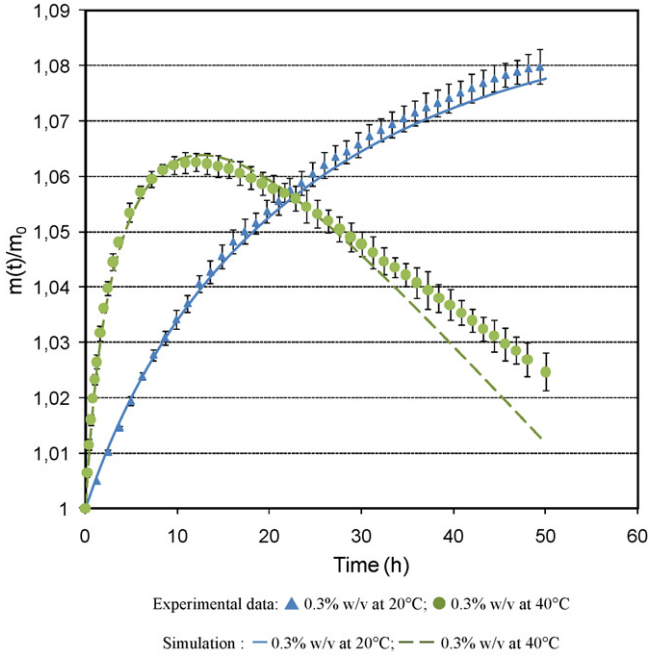

Fig. 20. Comparison between experimental data and simulated results for the additional chitin solution (M_w = 696,000 g/mol) – 43% RH at 20 °C and 40 °C – constant mass transfer coefficient: $k_{p10} = 1.55 \times 10^{-9}$ s/m and $k_{p20} = 3.04 \times 10^{-9}$ s/m (20 °C) and $k_{p10} = 2.15 \times 10^{-9}$ s/m and $k_{p20} = 4.2 \times 10^{-9}$ s/m (40 °C).

specific case since NMP molecules can migrate from the gas phase into the saturated saline solution due to the high affinity between NMP and water.

However, at 40 °C this deviation occurs after more than 30 h of experiments whereas the gelation time is less than 50 min, whatever the chitin source. It should be noted that the main objective of the model was to predict the solution composition during the gelation. Indeed, the gelation time is related to the solution composition and more precisely to the solvent quality. Since the agreement between the model prediction and the experimental data is good before the gelation time, the assumption of very low amount of NMP in the gas phase is relevant. Thus, the weak deviation observed after 30 h of experiments does not discredit the scientific analysis based on the relation between the solvent quality and gelation mechanisms.

4.3.2. Gelation time determined by rheological measurements

The gelation time was monitored by rheological measurements for the same concentration (0.3%, w/v). Even if the polymer concentration is lower, the gelation is much faster for the new chitin source (33 min at 20 °C) than for the batch 1 (175 min for the same temperature). Thus, the gelation time was greatly affected by the chitin chemical structure. Actually, both the higher degree of acetylation and the higher molecular weight favour gelation kinetics.

Previous studies showed that higher molecular weights lead to more rapid gelation kinetics for chitin [10] or konjac [43]. Gelation is due to the formation of junction zones between polymer chains. The probability of formation of these junction zones increases with increasing molecular weight [43]. In addition, the solubility of the polymer chains decreases, which favours the polymer–polymer interactions, thus leading to faster gelation [10].

Concerning the influence of the degree of acetylation, the presence of N-acetylglucosamine residues allows the formation of attractive hydrophobic interactions between chitin chains and thus favours gelation. In the case of chitin gels obtained by reacetylation of chitosan in a water/alcohol mixture, it was already demonstrated that increasing the DA leads to faster gelation kinetics [10].

5. Conclusion

In this study, a model incorporating coupled heat and mass transfer is implemented for predicting mass exchanges during the gelation induced by non-solvent vapours (VIPS-gelation process) of a chitin solution. The model was numerically resolved using finite element software.

The numerical results were validated using experimental data obtained by gravimetric measurements. Experiments were conducted in-line into a fabrication chamber where the process parameters where controlled. Two temperatures and three concentrations of chitin in the initial solution were tested, keeping constant the value of the relative humidity (43%). The comparison between experimental and numerical results pointed out that the model accurately predicts the mass variation of the polymer solution during the gelation process, without any adjustable parameters for fitting the curves. Mass transfer coefficients were only slightly overestimated at the beginning of the process due to the specific geometry used for the validation experiments.

Model predictions indicate that the transfer of water from the vapour phase to the solution is controlled by the operating conditions in the fabrication chamber, in particular the temperature. Because of higher internal resistance to mass transfer due to molecular diffusion, weak concentration gradients were predicted in the whole thickness of the solution for the lowest temperature (20 °C). At higher temperature (40 °C), the water concentration profiles exhibited higher gradients near the air/solution interface especially at the beginning of the process (two first hours). This phenomenon was explained in terms of higher driving force to mass transfer and thicker boundary layer in the gas phase that promote mass transfer resistance.

Then, the model was used for predicting the rate of change of the solvent quality, which is characterized by the molar ratio between the solvent (NMP) and the non-solvent (water). For a better understanding of the gelation process, the gelation time was also estimated by rheological measurements for various conditions of temperature and chitin concentration. Rheological results exhibited that increasing the temperature leads to a decrease of the gelation time, whatever the chitin concentration. The temperature was expected to have an impact on the mobility of the chitin chains and interchain associations and it was shown that a temperature increase enhances the mass transfer kinetics. The comparison of these results with the model predictions in terms of concentration profiles at the gelation time helped dissociating various effects. It was also pointed out that the temperature mainly affects the mass transfer rates. Besides, the model predictions exhibited that for both temperatures, the solvent quality required for gelation was strongly affected by the chitin concentration. Lower the chitin concentration in the initial solution, higher the water intake necessary to induce the gelation. Lastly, the presence of a gelation front visually observed during the gelation experiments was also explained in terms of concentration gradient in the thickness of the solution, from the top to the bottom. The influence of the chitin chemical structure was investigated on the mass exchanges and the gelation kinetics. It was exhibited that the chitin source does not affect the mass transfer rates for polymer concentrations in the range 0–5% (w/v), but higher the molecular weight and the DA, lower the gelation time.

Acknowledgment

The authors would like to address acknowledgments to the French National Agency of Research (ANR) which supports this study through the project PANSKIT (ANR-08-MAPR-0021-01).

References

[1] E. Knor, Chitin: a biomaterial in waiting, Curr. Opin. Sol. State Mater. Sci. 6 (2002) 313–317.
[2] S. Hirano, M. Zhang, M. Nakagawa, T. Miyata, Wet spun chitosan–collagen fibers, their chemical modifications, and blood compatibility, Biomaterials 21 (2000) 997–1003.
[3] Y. Shirosaki, T. Okayama, K. Tsuru, S. Hayakawa, A. Osaka, Synthesis and cytocompatibility of porous chitosan–silicate hybrids for tissue engineering scaffold application, Chem. Eng. J. 137 (2008) 122–128.
[4] H. Mansur, H.S. Costa, Nanostructured poly(vinyl alcohol)/bioactive glass and poly(vinyl alcohol)/chitosan/bioactive glass hybrid scaffolds for biomedical applications, Chem. Eng. J. 137 (2008) 72–83.
[5] B. Krajewska, Membrane-based processes performed with use of chitin/chitosan materials, Sep. Purif. Technol. 41 (2005) 305–312.
[6] F.A. Rutherford, W.A. Dunson, The permeability of chitin films to water and solutes, in: J.P. Zikakis (Ed.), Chitin, Chitosan and Related Enzymes, Academic Press, New York, 1984, pp. 135–143.
[7] A.M. Striegle, J.D. Timpa, Polysaccharides dissolved in Me_2NAc–LiCl by gel permeation chromatography, Carbohydr. Res. 267 (1995) 271–290.
[8] E. Yilma, M. Bengisu, Preparation and characterization of physical gels and beads from chitin solutions, Carbohydr. Polym. 54 (2003) 479–488.
[9] M. Vincendon, in: R.A.A. Muzzarelli, C. Jeuniaux, G.W. Gooday (Eds.), Chitin in Nature and Technology, Plenum Press, 1986, p. 343.
[10] L. Vachoud, N. Zydowicz, A. Domard, Formation and characterisation of a physical chitin gel, Carbohydr. Res. 302 (1997) 169–177.
[11] A. Montembault, C. Viton, A. Domard, Physico-chemical studies of the gelation of chitosan in a hydroalcoholic medium, Biomaterials 26 (2005) 933–943.
[12] Y. Chakrabandhu, C. Pochat-Bohatier, L. Vachoud, D. Bouyer, J.P. Desfours, Control of elaboration process to form chitin-based membrane for biomedical applications, Desalination 233 (2008) 120–128.
[13] H. Nagahama, N. Nwe, R. Jayakumar, S. Koiwa, T. Furuike, H. Tamura, Novel biodegradable chitin membranes for tissue engineering applications, Carbohydr. Polym. 73 (2) (2008) 295–302.
[14] M. Peter, P.T.S. Kumar, N.S. Binulal, S.V. Nair, H. Tamura, R. Jayakumar, Development of novel α-chitin/nanobioactive glass ceramic composite scaf-

folds for tissue engineering applications, Carbohydr. Polym. 78 (4) (2009) 926–931.
[15] D. Zhou, L. Zhang, S. Guo, Mechanisms of lead biosorption on cellulose/chitin beads, Water Res. 39 (16) (2005) 3755–3762.
[16] S. Liang, L. Zhang, J. Xu, Morphology and permeability of cellulose/chitin blend membranes, J. Membr. Sci. 287 (1) (2007) 19–28.
[17] N.L.B.M. Yusof, L.Y. Lim, E. Khor, Flexible chitin films: structural studies, Carbohydr. Res. 339 (2004) 2701–2711.
[18] C. Tsioptsias, C. Panayiotou, Foaming of chitin hydrogels processed by supercritical carbon dioxide, J. Supercrit. Fluids 47 (2) (2008) 302–308.
[19] A. Venault, D. Bouyer, C. Pochat-Bohatier, L. Vachoud, C. Faur, Modeling the mass transfers during the elaboration of chitosan-activated carbon composites for medical applications, AIChE J. (2009), 10.1002/aic.12078.
[20] J.S. Vrentras, J.L. Duda, Diffusion in polymer–solvent systems. II. A predictive theory for the dependence of diffusion coefficients on temperature, concentration, and molecular weight, J. Polym. Sci.: Part B: Polym. Phys. 15 (1977) 417–439.
[21] J.S. Vrentras, H.C. Duda, H.C. Ling, Self-diffusion in polymer–solvent systems, J. Poly. Sci.: Phys. 22 (1984) 459–469.
[22] J.M. Zielinski, J.L. Duda, Predicting polymer/solvent diffusion coefficients using free-volume theory, AIChE J. 38 (3) (1992) 405–415.
[23] Y. Yip, A.J. McHugh, Modeling and simulation of nonsolvent vapor-induced phase separation, J. Membr. Sci. 271 (2005) 163–176.
[24] S.S. Shojaie, W.B. Krantz, A.R. Greenberg, Dense polymer film and membrane formation via the dry-cast process. Part I. Model development, J. Membr. Sci. 94 (1994) 255–280.
[25] D. Bouyer, W. Werapun, C. Pochat-Bohatier, A. Deratani, Morphological properties of membranes fabricated by VIPS process using PEI/NMP/water system: SEM analysis and mass transfer modeling, J. Membr. Sci. 349 (2010) 97–112.
[26] G. Tkacik, L. Zeman, Component mobility analysis in the membrane forming system water/N-methyl-2-pyrrolidone/polyethersulfone, J. Membr. Sci. 31 (1987) 273–288.
[27] T. Boublik, V. Fried, E. Hala, The Vapor Pressure of Pure Substances: Selected Values of the Temperature Dependence of the Vapor Pressures in the Normal and Low Pressure Region, second ed., Elsevier, New York, 1984.
[28] S.H. Lee, Y.C. Bae, Thermal stress analysis for polyimide thin film: the effect of solvent evaporation, Macromol. Theory Simul. 9 (2000) 281–286.
[29] S. Alsoy, J.L. Duda, Modeling of multicomponent drying of polymer films, AIChE J. 45 (1999) 896–905.
[30] E.N. Fuller, K. Ensley, J.C. Giddings, Diffusion of halogenated hydrocarbons in helium, J. Phys. Chem. 75 (1969) 3679–3685.
[31] G.M. Kavanagh, S.B. Ross-Murphy, Rheological characterisation of polymer gels, Prog. Polym. Sci. 23 (1998) 533–562.
[32] H.H. Winter, F.J. Chambon, Analysis of linear viscoelasticity of a crosslinking polymer at the gel point, J. Rheol. 30 (2) (1986) 367–382.
[33] L. Payet, A. Ponton, F. Agnely, P. Colinart, J.L. Grossiord, Caractérisation rhéologique de la gélification d'alginate et de chitosane: effet de la température Rhéologie, vol. 2, 2002, pp. 46–51.
[34] J.A.L. Silva, M.P. Goncalves, Rheological study into the aging process of high methoxyl pectin/sucrose aqueous gels, Carbohydr. Polym. 24 (1994) 235–245.
[35] A.H. Clark, S.B. Ross-Murphy, Structural and mechanical properties of biopolymer gels, Adv. Polym. Sci. 83 (1987) 57–192.
[36] J.L. Doublier, B. Launay, G. Cuvelier, Viscoelastic properties of food gels, in: M.A. Rao, J.F. Steffe (Eds.), Viscoelastic Properties of Foods, Elsevier Applied Science, London, 1992, pp. 371–434.
[37] K. Almdal, J. Dyre, S. Hvidt, O. Kramer, Towards a phenomenological definition of the term "gel", Polym. Gels Networks 1 (1993) 5–17.
[38] K. Kataoka, H. Koyo, T. Tsuruta, Novel pH-sensitive hydrogels of segmented poly(amine ureas) having a repetitive array of polar and apolar units in the main chain, Macromolecules 28 (1995) 3336–3341.
[39] M.B. Huglin, J.M. Rego, Influence of temperature on swelling and mechanical properties of a sulphobetaine hydrogels, Polymer 32 (18) (1991) 3354–3358.
[40] J. Desbrieres, C. Martinez, M. Rinaudo, Hydrophobic derivatives of chitosan: characterization and rheological behaviour, Int. J. Biol. Macromol. 19 (1996) 21–28.
[41] S. Lack, V. Dulong, D. Le Cerf, L. Picton, J.F. Argillier, G. Muller, Hydrogels based on pullulan crosslinked with sodium trimetaphosphate (STMP): rheological study, Polym. Bull. 52 (2004) 429–436.
[42] A. Fatimi, J.F. Tassin, S. Quillard, M.A.V. Axelos, P. Weiss, The rheological properties of silated hydroxypropylmethylcellulose tissue engineering matrices, Biomaterials 29 (2008) 533–543.
[43] M. Yoshimura, K. Nishinari, Dynamic viscoelastic study on the gelation of konjac glucomannan with different molecular weights, Food Hydrocolloids 13 (3) (1999) 227–233.